IJME

Int. J. of Applied Mechanics and Engineering, 2026, vol.31, No.2, pp.50-71
DOI: 10.59441/ijame/218523

MHD FLOW OF WILLIAMSON-MICROPOLAR NANOFLUID OVER A NONLINEAR STRETCHING SHEET: A NUMERICAL INVESTIGATION

S. Kerrouche[1], R. Alouaoui[2], S. Ferhat[3], M.N. Bouaziz[4,5*]
[1]University of Medea, Mechanical Engineering, Biomaterials and Transport Phenomena, ALGERIA
[2]Faculté of Technology, Mechanical Engineering, Biomaterials and Transport Phenomena, ALGERIA
[3]University of Medea, Faculty of Technology, Process Engineering,
Biomaterials and Transport Phenomena Laboratory, ALGERIA
[4]Mechanical Engineering, Biomaterials and Transport Phenomena, ALGERIA
[5]University of Medea, Faculty of Technology,
Biomaterials and Transport Phenomena Laboratory, ALGERIA
E-mail: mn_bouaziz@email.com

This computational study examines a Williamson-micropolar nanofluid flow over a nonlinear stretching sheet subjected to a magnetic field. The Williamson fluid model, known for its ability to describe non-Newtonian shear-thinning behavior, is commonly applied in industrial polymers sheet extrusion. To highlight the influence of the involved parameters on the profiles an adequate mathematical model is formulated. Similarity transformations are used to convert the governing partial differential equations into a system of coupled nonlinear ordinary differential equations. The bvp4c solver of Matlab software is used to solve equations using the Lobatto III finite difference discretisation method with prior verification of the code developed. The impact of various physical parameters are explained and presented through graphs, tables and summarized in conclusion. The main result is that the relevant Williamson micropolar-nanofluid provides substantial improvement in thermal performance and reduced skin-friction can be gained. The values $[M, K, \lambda, Sc, Pr, Nb, Nt]=[0.5, 2.0, 0.1, 1.0, 3.0, 0.15, 0.15]$ appear to be a good trade-off between reasonable heat exchange and less flow resistance. Optimization of the above-mentioned parameters can also be performed for various combinations that may be useful for a specific application.

Keywords: stretching sheet, Williamson, nanofluid, micropolarity, magnetohydrodynamic.

1. Introduction

As the world faces growing energy demands and environmental challenges, advances in heat transfer science will play a crucial role in shaping energy systems that are cleaner, more efficient, and better suited to the needs of future generations. From power generation to energy storage and beyond, improving heat transfer continues to be an important factor in advancing the science of energy. A first response to this challenge was made possible by the fabrication of metallic nanoparticles to improve the thermal conductivities of conventional fluids. Subsequently, nanofluids have been applied to almost all branches of technology and more recently to non-Newtonian basic fluids. Nowadays, there is a growing interest in studies involving the use of these fluids in combination with magnetohydrodynamics. These ongoing efforts are part of the intensification and improvement of thermal exchanges encountered in various industrial sectors.

A moving surface interacting with a fluid characterizes many engineering processes for the transformation of basic products. For example, polymer sheets by extrusion are produced from an industrial machine based on a moving surface in order to transform molten plastic. Optimizing the production speed and system performance is highly dependent on dynamic and thermal transfers. Thus, the use of the stretching sheet model is of fundamental task for analyzing the induced effects on the finished product or for the development

* To whom correspondence should be addressed

of adequate cooling systems. Williamson fluids characterized by their non-Newtonian behavior, exhibit rheological properties that enhance their application in heat transfer and energy systems.

These specific fluids demonstrate shear-thinning behavior, meaning their viscosity decreases with increased shear rate which improves their flow characteristics. For example, solutions and melts of high molecular weight polymers used in extrusion belong to the class of pseudoplastic materials. Based on a choice of minimum and maximum viscosities, the behavior of such rheology was mathematically modeled by Williamson [1] and experimentally validated. The Williamson model is simpler to implement than those of Cross or Carreau-Yasuda and its applications are relevant to complex fluid flows with pronounced non-Newtonian behavior. The Williamson base fluids containing nanoparticles can serve as lubricants, providing better adaptation to changing friction conditions and reduced mechanical wear. In advanced medicine, and in the case of treatment by magnetotherapy, the Williamson fluid is preferred for the in-depth knowledge of blood circulation in irregular arteries. Combined with a nanofluid, it is becoming an increasingly popular candidate for innovative systems for cooling heat exchangers. The Rivlin-Ericksen model serves as a comprehensive framework that can include Williamson fluids as a specific case. Several models contribute significantly to the understanding of non-Newtonian fluid dynamics, particularly in applications requiring the analysis of viscoelastic materials. Bishnoi and Kumar [2] studied stability of Rivlin-Ericksen category of nanofluid saturated in a continuous medium bounded by infinite horizontal plates. Carapau [3] analyses the unsteady flow of an incompressible generalized second-order fluid in a straight rigid tube with circular cross-section of constant radius. A power law model is considered. The two-dimensional flow of a Williamson fluid model across a stretched sheet was studied by Nadeem and Hussain [4]. They developed the governing equations for the pseudoplastic Williamson fluid and then made them simpler approach by similarity transformations. The implications of heat transmission on the Williamson fluid across a porous surface that extends exponentially were examined by Nadeem and Hussain [5]. Salawu [6] analysed numerically the implication of a stagnation-point flow together with the influence of activation energy. As result, increasing the Williamson parameter reduced skin friction.

The utilization of nanofluids, which are engineered by suspending nanoparticles in a base fluid, offers significant benefits in heat transfer and energy applications. Review of Dey and Sahu [7] cited wide and varied applications and conclude that nanofluids will play a major role in the targeted areas in the near future. Nanofluids exhibit enhanced thermal conductivity and increased heat transfer coefficient, resulting in better heat transfer performance systems, like heat exchangers and cooling devices. This process can reduce the required flow rates, thereby lowering pumping power and energy costs. Recent research on nanofluids that employs the Williamson model has significantly advanced our understanding of their thermal and flow characteristics particularly in the enhancing heat transfer applications. Various researchers have investigated the impacts of different types of nanoparticles and their concentrations, revealing that these factors play a strong role in optimizing the thermal performance. For each combination nanoparticle/base fluid, Sharma *et al.* [8] noted that particle shape, its concentration, shear rate range, surfactant and magnetic field significantly affect the rheological behaviour of any nanofluid. For examples, TiO2/water, Fe3O4/polyethylene glycol (PEG), Fe3O4/polyethylene glycol (PEG) without dispersant displayed at *25°C*, showed shear thinning behavior. Very strong thinning behavior is observed with specific dispersant. Over a stretching sheet, Anjali and Devi [9] explicated the role of Brownian motion and thermophoresis effects on the hydromagnetic nanofluid flow. Shahzed *et al.*[10] studied the thin film flow of a nanofluid. Saif and Mohammed [11] consider a curved stretching sheet in interaction with porous media saturated by a nanoliquid. Waqas *et al.* [12] examined hybrid nanofluid with blood-base fluid flow in stenotic artery. More recently, Mohammed and Haider [13] present Reiner-Rivlin nanofluid flow over a stretching sheet.

Nanofluids can exhibit micropolar characteristics due to the presence of suspended nanoparticles. They enhanced thermal conductivity but also introduce complexities in flow behavior. These fluids can demonstrate rotational effects and shear-thinning properties, making them valuable in applications. Research on micropolar-nanofluids focuses on the microrotation that arise from the microstructure and the presence of nanoparticles. When a rotational field is developed in a fluid, micropolarity becomes significant. The existence of rigid particles in colloidal suspensions or the addition of nanoparticles for nanofluids is a natural condition for micropolarity. It is essential to take it into account for lubricants containing solid particles and for studies on

nanofluids. Eid and Mabood [14] look into the effects of heat sources/sinks and thermal radiation for a micropolar-nanofluid in porous medium interacting with an expanding sheet. Their findings revealed that a reduction is observed in both flow velocity and temperature when the suction parameter increased. However, an increase in the injection parameter enhances both flow velocity and temperature. Ramesh *et al.*[15] examined the squeezing flow of a Casson-micropolar nanofluid focusing on the impacts of injection/suction and slip effects. Their study provides insights into how these parameters influence the nanofluid's behavior contributing to a better understanding of its rheological properties and applications in engineering processes. Almakki *et al.*[16] studied a micropolar-nanofluid finding that thermal diffusion significantly contributes to entropy generation. Additionally, they found that efficiency increases with increasing Reynolds and Brinkman numbers.

Due to its important role in enhancing heat transfer, control flow behavior magnetohydrodynamics (MHD) is a good tool for nanofluids for improving thermal stability. Applying it optimizes the flow patterns and reduces turbulence leading to better convective heat transfer. Numerous authors worked based on physical phenomenon under magnetic field. Reddy *et al.* [17] studied Eyring-Powell flow with variable wall thickness, Kumar *et al.* [18] consider nanofluid flow in 3D while Khan *et al.* [19] were interested on variable rotating surface. Porous stretching sheet study is presented by Odesola *et al.* [20]. Dang *et al.* [21] used a permeable stretching sheet in their analysis whilst Ahmed *et al.* [22] deduced similarity variables for Williamson flow over a nonlinear stretching sheet (NSS). Recently, Jauhri and Mishra [23] studied MHD effect on nonlinear stretching sheet. Past on NSS, cross diffusions effects of Williamson fluid flow in permeable medium are discussed, Iqbal *et al.* [24]. Entropy generation analysis is presented by Mesbah *et al.* [25]. Study on Magnetized peristaltic transport is given by Iqbal *et al.* [26]. Irfan and Mohammed [27] used the Carreau model to conduct a numerical simulation of bio-convection radiative heat transport nanofluid flow. The same rheology is invoqued by Iqbal *et al.* [28] to determine the thermal enhancement in solar aircraft. For magnetohydrodynamic flow of hybrid nanofluid over a curved stretching surface non-similar analysis is established by Iqbal *et al.* [29]. Others studies have delved into the intriguing interplay between MHD and nanofluids. Alouaoui *et al.* [30] studied the impact of magnetic field, suction/injection and stability on heat transfer within a laminar boundary layer flow of micropolar nanofluids adjacent to a moving vertical permeable plate. They found that microrotation of suspended nanoparticles and the presence of the magnetic field contribute to better heat transfer, provided that the micropolar nanofluids maintain good chemical stability. The magnetohydrodynamic stagnation point flow of a Williamson hybrid nanofluid across a porous extended sheet is carried out by Vinodkumar Reddy *et al.* [31]. Similar to this, Jangid *et al.* [32] explicited Nusselt and local Sherwood numbers using Williamson nanofluid flow over an exponentially stretched surface with MHD impact. In another case, Sharma and Jain [33] conducted an investigation about the unsteady Williamson fluid flow towards vertical parallel porous plates through porous media. They found that the magnetic field have a significant effect on the fluid velocity at the solid–fluid interface. A magnetic Williamson hybrid nanofluid in a porous media around an inclined stretched cylinder is considered by Nabwey *et al.* [34]. Chandan *et al.*[35] explored double-diffusive convection problem by applying MHD effect on Williamson fluid flowing in a porous medium. Butt *et al.* [36] used radial basis kernel harmony method for MHD-Williamson nanofluid problem along a stretchable surface under the influence of chemical reaction and thermal radiation. Jeffrey-Williamson fluid gives lower skin friction, Nusselt and Sherwood numbers than Oldroyd-B fluid concluded Rashad *et al.*[37]. In the same context Rashad *et al.*[38] examine how heat variation affects Williamson hybrid nanofluid under MHD. This last study focuses on convective boundary conditions within a curved coordinate porous medium. Paul *et al.*[39] found that the hybrid nanofluid exhibits an absolute skin friction that may exceed the mono-nanofluid around *31%*. Another research on Maxwell hybrid nanofluid was diffused by Jeelani *et al.*[40] showing the effect of magnetic field on velocity and temperature profiles. A numerical study is conducted by Das *et al.*[41] to scrutinize the behavior of a Darcy-Forchheimer electromagnetohydrodynamic (EMHD) flow of a sodium-based Williamson fluid. The results showed that the rate of thermal transport adjacent to the vertical cylindrical wall is influenced by thermo-convective effects. They demonstrate an average increase of *47%*. when using the SA-based Williamson hybrid nanofluid, in contrast to the standard Williamson fluid.

In light of the explored literature, an investigation of a specific combination will be carried out for a possible improvement of the quantities of engineering interest. For this purpose, the current work inquires to heat transfer reached using Williamson micropolar-nanofluid over horizontal nonlinear stretching plate

subjected to magnetic field. The combination of pseudoplastic rheology decreasing fluid viscosity with increasing shear rate, enhanced by thermal conductivity improved by addition of nanoparticles is expected as well tandem. With micropolarity included and under magnetic field control, the present work fills a significant gap in the scientific literature dedicated for nonlinear stretching processes. So, we propose to open up a beneficial and possible innovative avenue. The significance of this study lies in its contribution to the theoretical foundations inspiring new advances in applied fluid dynamics and thermal engineering. Potential practical implications include the optimal design of energy-efficient thermal management systems for industry and biomedical engineering.

Solving a complicated simulation problem requires a specific mathematical framework to modeling the multiple mechanisms involved and an accurate numerical method to solve the developed mathematical system. The momentum, angular momentum, thermal and volume fraction of the nanoparticles boundary layers equations are turned into ordinary differential equations via similarity transformations. These equations are then numerically solved with MATLAB's bvp4c tool. The influence of the couples $(M-K)$; $(M-\lambda)$; $(Nb-K)$; $(Nb-\lambda)$; $(Nt-K)$ and $(Nt-\lambda)$ on the profiles are shown using selected data through graphs. Important values of engineering quantities are analyzed. It is important to proceed in this way because of the number of couplings induced by this complex combination.

2. Problem description

2.1. Assumptions and illustration

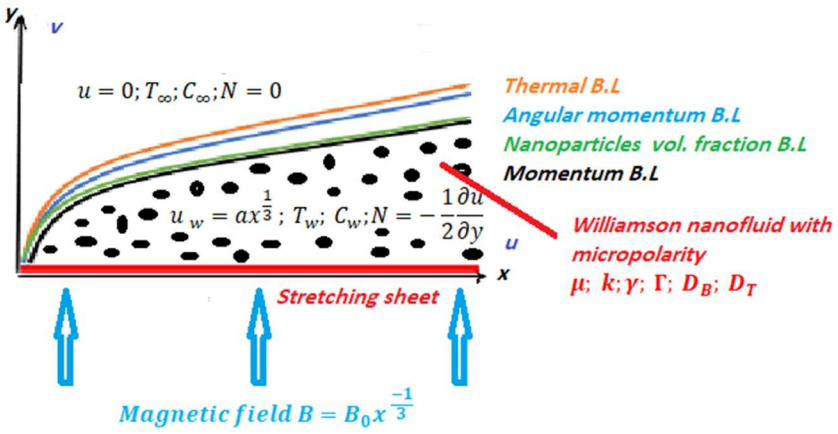

Fig.1. Schematic physical problem.

Examine a Williamson micropolar-nanofluid (WMN) with two-dimensional steady flow on a nonlinear stretched surface (NSS), where x and y axis are along and perpendicular to the surface, respectively. u and v are the velocities along the x-axis and y-axis**.** Some concrete assumptions are made to simplify the problem:

- The stretching sheet have a variable velocity in accordance with the position.
- Two equal and opposite forces are applied along the x-axis to produce stretching, keeping the origin fixed.
- WMN flow is generated due to the stretching sheet.
- The nanofluid adheres to the sheet as a non-slip condition
- The flow is bidimensional and laminar.
- The basic-nanofluid is assumed pseudoplastic fluid with incompressible Williamson rheological behavior.
- The Buongiorno' model including Brownian motion and thermophoresis mechanisms is applicable.
- The microstructures and nanoparticles substructure undergo to rotation independent of their linear velocities.
- The complex nanofluid is subjected to a variable locally magnetic field B with no Hall effects, is applied perpendicularly to the direction of flow.

- Heat dissipation from magnetic field is assumed negligible.
- A constant volume fraction of the nanoparticles at the interface is supposed actively maintained.
- Conditions of application of classical heat transfer laws are satisfied.
- No radiation or thermal disturbances are happening between the nanofluid and the sheet.

Figurate 1 presents a simplified illustration of the nonlinear stretching sheet with the velocity $u_w(x)$, under magnetic field $B(x)$. All the boundary conditions are reported in Fig.1.

2.2. The Williamson fluid model

The basic formulation of the Williamson model is expressed by the extra stress tensor, second component of the Cauchy stress tensor, as:

$$\tau = \left[\mu_\infty + \frac{(\mu_0 - \mu_\infty)}{1 - \Gamma\dot{\gamma}} \right] \boldsymbol{A}_1 . \tag{2.1}$$

Where μ_0 and μ_∞ are the viscosities at zero shear rate and at infinity shear rate, respectively. Γ is a strictly positive time constant, called the relaxation time. $\boldsymbol{V}$ being the velocity field, *grad* the gradient operator and T refers as transpose matrix, then $\boldsymbol{A}_1$ the first Rivlin-Ericksen tensor is:

$$\boldsymbol{A}_1 = grad\,\boldsymbol{V} + grad\,\boldsymbol{V}^T . \tag{2.2}$$

It should be noted that the present Williamson model is a restriction of the full constitutive equation for second-grad fluid including in addition elasticity and cross-diffusion terms, Mohyuddin [42], Rivlin and Ericksen [43].

The shear rate $\dot{\gamma}$ is:

$$\dot{\gamma} = \sqrt{\frac{1}{2} \operatorname{trace} \boldsymbol{A}_1^2} . \tag{2.3}$$

In the conditions, $\mu_\infty = 0$ and $\Gamma\dot{\gamma} < 1$, the extra shear stress will be:

$$\tau = \mu_0 \left[1 + \Gamma\dot{\gamma} \right] \boldsymbol{A}_1 . \tag{2.4}$$

For a bidimensionnel flow (x, y), the rate of shear is, [4]:

$$\dot{\gamma} = \left[\left(\frac{\partial u}{\partial x} \right)^2 + \frac{1}{2} \left(\frac{\partial u}{\partial y} + \frac{\partial v}{\partial x} \right)^2 + \left(\frac{\partial v}{\partial y} \right)^2 \right]^{\frac{1}{2}} . \tag{2.5}$$

Applying the boundary layer approximations to the components of the tensor, Nadeem *et al.* [4], the extra shear stress in relation to $\frac{\partial u}{\partial y}$ become:

$$\tau = \mu_0 \frac{\partial u}{\partial y} + \frac{\Gamma}{\sqrt{2}} \left(\frac{\partial u}{\partial y} \right)^2 . \tag{2.6}$$

3. Mathematical analysis

Transitioning from a physical model to a mathematical model involves analyzing the physical phenomena. By appropriate laws the governing equations can be developed.

For the defined problem, the governing conservation equations of mass, momentum and angular momentum, energy and nanoparticles volume fraction can be expressed as:

$$\frac{\partial u}{\partial x}+\frac{\partial v}{\partial y}=0, \tag{3.1}$$

$$u\frac{\partial u}{\partial x}+v\frac{\partial u}{\partial y}=\left(\frac{\mu+\kappa}{\rho}\right)\frac{\partial^2 u}{\partial y^2}+\sqrt{2}\Gamma\upsilon\frac{\partial u}{\partial y}\frac{\partial^2 u}{\partial y^2}-\sigma\frac{B^2}{\rho}u+\frac{\kappa}{\rho}\frac{\partial N}{\partial y}, \tag{3.2}$$

$$j\rho\left(u\frac{\partial N}{\partial x}+v\frac{\partial N}{\partial y}\right)=\gamma\frac{\partial^2 N}{\partial y^2}-\kappa\left(2N+\frac{\partial u}{\partial y}\right), \tag{3.3}$$

$$u\frac{\partial T}{\partial x}+v\frac{\partial T}{\partial y}=\alpha_{nf}\frac{\partial^2 T}{\partial y^2}+\frac{(\rho c)_p}{(\rho c)_f}\left[D_B\frac{\partial C}{\partial y}\frac{\partial T}{\partial y}+\frac{D_T}{T_\infty}\left(\frac{\partial T}{\partial y}\right)^2\right], \tag{3.4}$$

$$u\frac{\partial C}{\partial x}+v\frac{\partial C}{\partial y}=\frac{D_T}{T_\infty}\frac{\partial^2 T}{\partial y^2}+D_B\frac{\partial^2 C}{\partial y^2}. \tag{3.5}$$

In this context, T represents the temperature within the boundary layer, while N denotes the component of the microrotation vector that is normal to the *x*-*y* plane. Other parameters and quantities are defined in the nomenclature. Following the approach taken by several recent authors, as Long Hsiao [44], let's assume that the spin gradient viscosity is given by the expression $\gamma=(\mu+\kappa/2)j$.

The boundary conditions are:

$$\text{at}\quad y=0;\quad u=u_w=ax^{\frac{1}{3}}\ (a\ \text{is constant}),\quad v=0,\quad T=T_w,\quad C=C_w,\quad N=-n\frac{\partial u}{\partial y} \tag{3.6}$$

$$\text{for}\quad y\to\infty;\quad u=0,\quad T\to T_\infty,\quad C\to C_\infty,\quad N\to 0. \tag{3.7}$$

In this case *n* is taken equal to $1/2$, considering weak concentrations as noted in [44]. For simplicity, here active condition C_w is considered rather than zero mass flux [45].

This process entails the introduction of dimensionless quantities and similarity variables, following the methodology, Yacob and Ishak [46].

$$\eta=x^{-\frac{1}{3}}(a/\upsilon)^{\frac{1}{2}}y,\quad N=u_w(u_w/x\upsilon)^{\frac{1}{2}}h(\eta). \tag{3.8}$$

For the dimensionless temperature and the volume fraction of nanoparticles:

$$\theta=\frac{T-T_\infty}{T_w-T_\infty},\quad \varphi=\frac{C-C_\infty}{C_w-C_\infty}. \tag{3.9}$$

It is expected that these new variables will lead to similarity, otherwise other techniques must be used. In these changes, $h(\eta)$ signifies the dimensionless microrotation. The stream function $f(\eta)$ is defined:

$$u=\frac{\partial f}{\partial y} \quad \text{and} \quad v=-\frac{\partial f}{\partial x} \quad \text{leading to:}$$
$$u=ax^{\frac{1}{3}}f'(\eta) \quad \text{and} \quad v=-\frac{(\upsilon a)^{\frac{1}{2}}}{3(x)^{\frac{1}{3}}}\left(2f(\eta)-\eta f'(\eta)\right). \tag{3.10}$$

The nonlinear partial differential, Eqs. (3.1-3.5), with boundary conditions, Eqs. (3.6-3.7) are coupled and present highly nonlinear system that cannot be solved analytically. To address this task, the similarity technique on Eqs. (3.1-3.7) is applied to generate a nonlinear ordinary differential equations system.

By employing the above transformation, Eqs. (3.8-3.10), the governing equations with the corresponding boundary equations take the following form:

$$f'^2-2ff''-3(1+K)f'''-\lambda f''f'''+Mf'-3Kh'=0, \tag{3.11}$$

$$\frac{2}{3}fh'+\left(1+\frac{K}{2}\right)h''-K(2h+f'')f'=0, \tag{3.12}$$

$$2Prf\theta'+3\theta''+3Nb\theta'\phi'+3Nt\theta'^2=0, \tag{3.13}$$

$$\frac{2}{3}Scf\phi'+\frac{Nt}{Nb}\theta''+\phi''=0. \tag{3.14}$$

The boundary conditions become

$$\eta=0: f'(0)=1; \quad f(0)=0; \quad h(0)=-\frac{1}{2}f''(0); \quad \theta(0)=\phi(0)=1, \tag{3.15}$$

$$\eta\to\infty: f'(\infty)\to 0; \quad h(\infty)\to 0; \quad \theta(\infty)\to 0; \quad \phi(\infty)\to 0. \tag{3.16}$$

The above identified dimensionless parameters are: $K=\kappa/\mu$ the material parameter, $Pr=\nu/\alpha_{nf}$ the Prandlt number, and $\lambda=3\sqrt{2}\,\Gamma a\left(a/\upsilon\right)^{\frac{1}{2}}$ the Williamson parameter. $Sc=PrL_n=\nu/D_B$ the Schmidt number, and $L_n=\alpha_{nf}/D_B$ the nanofuid Lewis number.

$M=3\sigma\left(\frac{B_0^{\,2}}{\rho a}\right)$ the magnetic parameter, $Nb=(\rho c)_p D_B(C_w-C_\infty)/(\rho c)_f\,\alpha_{nf}$ the Brownian motion parameter, and $Nt=(\rho c)_p D_T(T_w-T_\infty)/(\rho c)_f\,T_\infty\alpha_{nf}$ the thermophoresis parameter.

To complete the present formulation, the physical quantities of interest are defined as:

$$C_f=\frac{\tau_w}{\rho u_w^2}, \quad Nu_x=\frac{x\,qh_w}{T_w-T_\infty}, \quad Sh_x=\frac{x\,qm_w}{C_w-C_\infty}. \tag{3.17}$$

Which are the local skin friction, Nusselt number, and Sherwood number of nanoparticles, respectively. The shear stress τ_w, heat flux qh_w and nanoparticles mass flux, qm_w, all at the wall, are related to primitive variables by:

$$\tau_w = \left[\mu\left(\frac{\partial u}{\partial y}\right) + \frac{\Gamma}{\sqrt{2}}\left(\frac{\partial u}{\partial y}\right)^2 + \kappa N \right]_{y=0},$$

$$qh_w = \left[-\left(\frac{\partial T}{\partial y}\right) \right]_{y=0} \quad \text{and} \quad qh_w = \left[-\left(\frac{\partial C}{\partial y}\right) \right]_{y=0}. \tag{3.18}$$

In dimensionless form:

$$C_f = \left[f'' + \frac{\lambda}{6} f''^2 + Kh \right]_{\eta=0}, \quad \frac{Nu_x}{Re_x} = -\theta'(0) \quad \text{and} \quad \frac{Sh_x}{Re_x} = -\phi'(0). \tag{3.19}$$

Where $Re_x = u_w \left[\frac{x^{\frac{2}{3}}}{av} \right]^{\frac{1}{2}}$ is the local Reynolds number.

4. Results and discussions

4.1. Solution method and accuracy

In a first step, different discretization methods can be proposed for the nonlinear and coupled system of partial differential equations, Eqs. (3.1-3.7), such as finite differences, finite elements, finite volumes, spectral methods and their numerous variants.

The initial step to solve Eqs. (3.11-3.16) is to write them to suitable following expressions according to the procedure of bvp4c @Matlab:

$$\begin{cases} f', \\ f'' \\ \left(f'^2 - 2ff'' + Mf' - 3Kh'\right) / \left[3(1+K) + \lambda f''\right], \\ h', \\ \left(-2/3\right) fh' + K\left(2h + f''\right) f') / \left(1 + K/2\right), \\ \theta', \\ -\dfrac{2Prf\theta + 3Nb\,\theta'\phi' + 3Nt\theta'^2}{3}, \\ \phi', \\ \left[-2/3\,Scf\phi' + Nt/3Nb\left(2Prf\theta + 3Nb\,\theta'\phi\text{ ^ }' + 3Nt\theta'\text{^ }2\right)\right] \end{cases},$$

and for the boundary conditions

$$\begin{cases} f(0), \\ f'(0)-1, \\ h(0)+(1/2)f''(0), \\ \theta(0)-1, \\ \phi(0)-1, \\ f'(\infty), \\ h(\infty), \\ \theta(\infty), \\ \phi(\infty). \end{cases}$$

Therefore, the nonlinear system of algebraic equations is generally solved numerically, in a second step, via iterative approaches based on Newton's method. Although the local search schemes such as the Levenberg propagation scheme derived from the Levenberg-Marquardt method are rather used in the context of neural networks, [47-48], it is not suitable for large systems where the conditioning of the matrices is not guaranteed, especially in complex rheology as is the case here. However, other specific methods can be applied, analytical or semi-analytical approaches, as used in [49-50].

As mentioned above, here the *2-D* system is transformed via the *1-D* similarity technique whose discretization and then resolution is precise, simpler and inexpensive using a robust computational algorithm.

This problem is then well-suited for numerical solutions, particularly using finite difference discretisations used by the software Matlab built in bvp4c techniques. Numerical Runge-Kutta methods can effectively address the ordinary differential equations, leading to a manageable algebraic system. bvp4c of @MATLAB provide more powerful tool and functions that facilitate the computation and visualization of solutions. The Runge-Kutta list is broadened with additional classes, including embedded methods, which differ from the implicit Lobatto family used in bvp4c. Focusing on this better discretisation and local truncation error estimates for individual steps rather than global estimates, the accuracy of bvp4c is much better. Throughout each integration subinterval, solution estimates are calculated using the midpoint quadrature rule at both the beginning and end.

Afterwards, these equations are implemented in respect to bvp4c coding. The above systems of derivatives functions and residuals boundary conditions are carefully written. The replacement of bounded domain $[0,\infty]$ is $[0,6]$, corresponding to a fixed value of η_{max}. It has found that the corresponding boundary condition is fullfilled and not causing beyond significant variations. The computation were performed by a choice of initial solution vector, a mesh such $\Delta\eta = 0.001$ and a fixed 10^{-5} convergence criterion was selected to ensure an accepted accuracy.

4.2. Validation

A test of the program built on the basis of the specified system is undertaken without micropolarity and magnetic field $(K = M = 0)$ and considering a classical Newtonian fluid without nanoparticles ($\lambda = 0$, $Nb = 10^{-5}$ and $Nt = 0$. The results – not shown here for brevity – and compared with those of the classical literature, show a total agreement. For $-\theta'(0)$, more calculations are carried out, in the same conditions to compare results performed by the present code with results of Ahmed *et al.* [22]. To do this, $M = K = 0$, $Le = 4$, and Nb, Nt take the following values 2 and 1, in order to adapt them to the relations $Nb = Nc / Le$ and $Nt = Nb / Nbt$, in [22]. Table 1 presents this comparison for a nonlinear stretching sheet. The implemented code is therefore error-free.

Table 1. Compared results $(-\theta'(0))$ for a nonlinear stretching sheet $\left(u_w = ax^{\frac{1}{3}}\right)$, $M = K = 0$, $Le = 4$, $Sc = 0.5$, $Nb = 2$, $Nt = 1$.

λ	Pr	Ahmed *et al.* [22] shooting method-bvp4c	Present code bvp4c method
0	*0.5*	*0.319*	*0.318501*
0.2	*0.5*	*0.318*	*0.317724*
0.4	*0.5*	*0.317*	*0.316813*
0.2	*0.2*	*0.231*	*0.231213*
0.2	*0.6*	*0.347*	*0.346835*
0.2	*1.2*	*0.521*	*0.521121*

Then, computer simulations were run to perform the velocity, microrotation, temperature and concentration of nanoparticles profiles. The data involved for K, M, λ, Nb, Nt are taken based on the large literature. The sensibility of the skin friction coefficient (C_f) and Nusselt number (Nu) on the parameters coefficients are calculated, using Eq.(3.19).

4.3. Effect of material parameter K and magnetic parameter M on the profiles

The material parameter K measures the degree of interaction between the microrotation of microstructures or torque effects, and the translational motion of the overall nanofluid. An increase in the material parameter K, which represents additional viscosity due to the micropolarity leads to significant thicker boundary layer observed in Fig.2. M quantifies the intensity of the effect of the magnetic field applied to the conductive nanofluid. Transverse magnetic field causes a resistive force, called Lorentz force that reduces strongly the movement of the nanofluid. Thus, an increase in the magnetic parameter M, in the same figure, acts against the fluid motion, further reducing velocity with higher gradients.

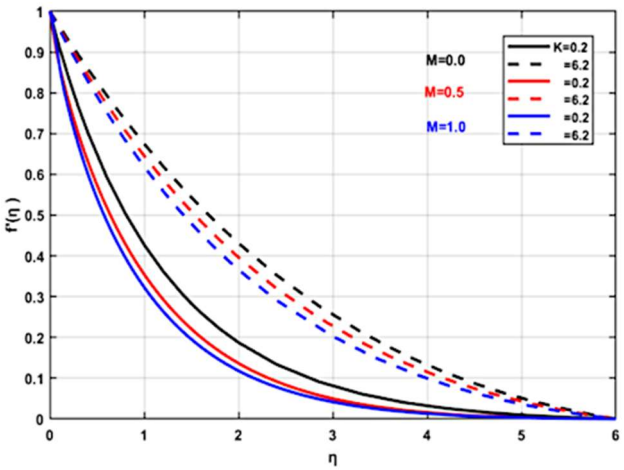

Fig.2. Velocity profiles $f'(\eta)$ for different values of M and K ($\lambda = 3.0$, $Sc = 1.0$, $Pr = 1.0$, $Nt = 0.1$, $Nb = 0.1$).

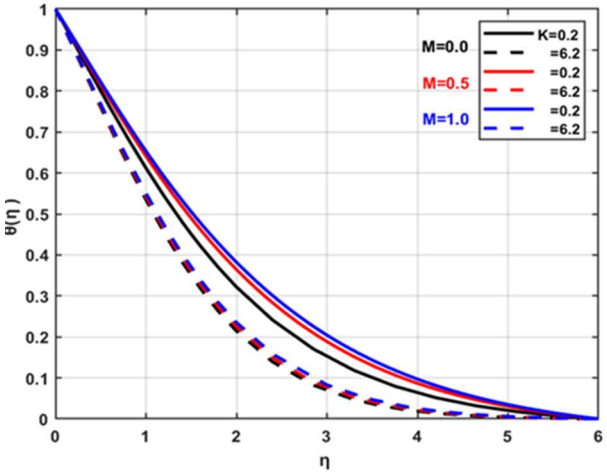

Fig.3. Temperature profiles $\theta(\eta)$ for different values of M and K ($\lambda = 3.0$, $Sc = 1.0$, $Pr = 1.0$, $Nt = 0.1$, $Nb = 0.1$).

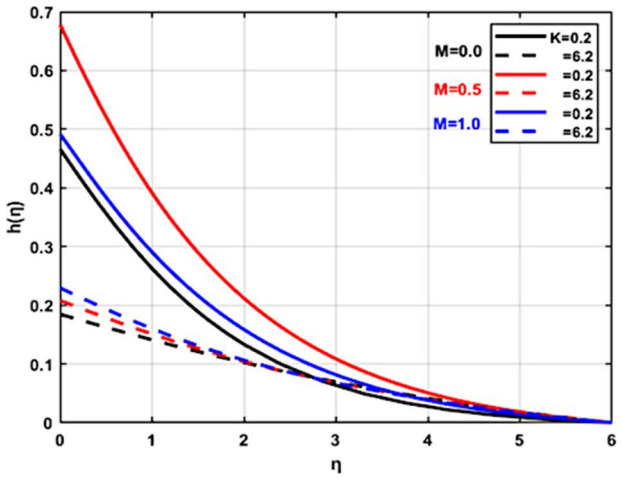

Fig.4. Microrotation profiles $h(\eta)$ for different values of M and K ($\lambda = 3.0$, $Sc = 1.0$, $Pr = 1.0$, $Nt = 0.1$, $Nb = 0.1$).

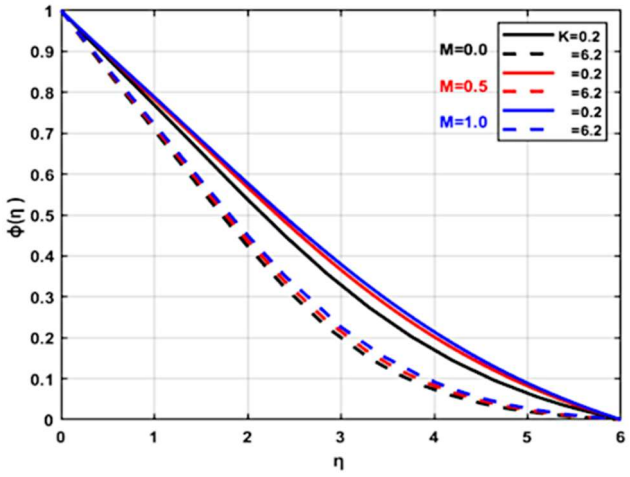

Fig.5. Concentration profiles $\phi(\eta)$ for different values of M and K ($\lambda = 3.0$, $Sc = 1.0$, $Pr = 1.0$, $Nt = 0.1$, $Nb = 0.1$).

The nanofluid has an increased capacity to store heat via microscopic effects. Increasing both K and M explains an increase in the temperature in the boundary layer, Fig.3. The temperature is raised sensibly by M for low values of K, due to heat dissipation in the middle of the boundary layer. It noticed that the impact of K and M have reversed roles on the velocity and temperature. The microrotation decreases largely with rasing K near the stretching sheet, Fig.4. This can be attributed to the relatively weak activity of the microstructures imposed as boundary condition. These aspects of curves can be improved greatly by medium value of M. For example, when $M = 0.5$ and $K = 0.2$, a maximum microrotation is noted near the sheet probably due to coupling actions and their reverse effects. It is found in Fig.5, that the concentration profile changes in amplitude due to micropolarity, which influences particle diffusion. On the same figure, the low heat dissipation can be advanced to explain the little changes in the uniform concentration nanoparticles profiles with M. High K makes the concentration profile thickness thinner. These effects are consistent with the graphs established in [22].

4.4. Effect of Williamson parameter λ and magnetic parameter M on the profiles

The Williamson parameter λ expresses the deformation response of the nanofluid to a shear rate. λ growing corresponds to pseudoplastic behavior of the Williamson nanofluid than the viscous behavior. In Fig.6, due to the decreased viscous resistance, the nanofluid flows more easily and the velocity profile becomes flatter at the center due to an improvement in the velocity gradient. For the same reason, the boundary layer thickness decreases because the transition from stretching sheet velocity to free velocity is faster. More is intensity of the applied magnetic field M more is reductions in velocity profiles as mentioned previously. The combined increase of M and λ has the effect of increasing the velocity gradients. As said, M introduces additional resistance to fluid motion but more heat dissipation. Overall, the combined effects of increased λ and M result in slower fluid flow, reduced mixing capabilities, does not greatly alter temperature distributions and solute concentrations depending on the level of heat dissipation. Concisely, higher values of λ indicate a greater tendency for shear-thinning. As λ increases, the fluid exhibits less pronounced resistance to flow. This is because the internal structure of the Williamson nanofluid becomes less rigid under strong shear stress, leading to a great ability to deform and flow. Causing less viscosity and thermal dissipation when λ increases, the variations of the temperature profile with λ are slightly higher, under this value of Pr, Fig.7. Obviously, the thermal boundary layer become more thicker. The microrotation profiles which play a major role near the stretching sheet and the nanofluid are seen the strong rotation of the microstructures near it, Fig.8. This can be

explained by greater ease of turning in the presence of less resistance. Additionally, lower viscosity resulting from high shear rates promotes better particle diffusion causing higher concentration values throughout the profile as it seems in Fig.9. For the velocity, temperature and nanoparticle concentration, these trends are similar to those found in [5, 22], regarding λ and M .

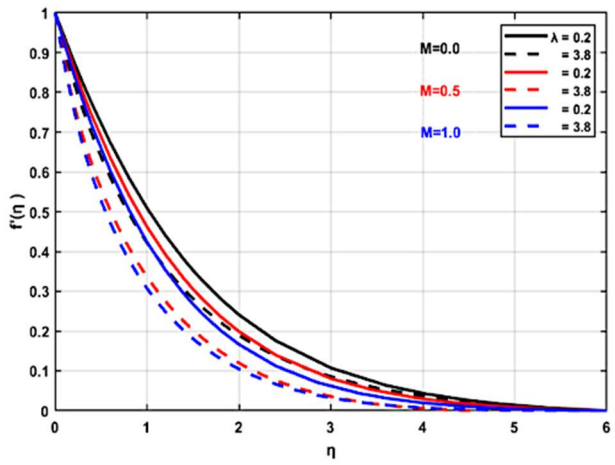

Fig.6. Velocity profiles $f'(\eta)$ for different values of M and λ ($K=0.4$, $Sc=1.0$, $Pr=1.0$, $Nt=0.1$, $Nb=0.1$).

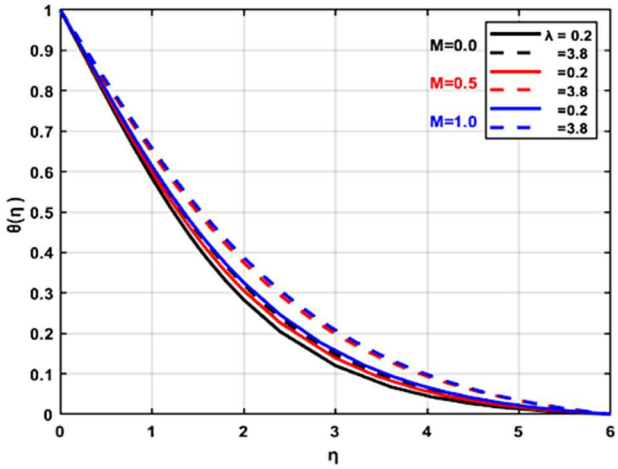

Fig.7. Temperature profiles $\theta(\eta)$ for different values of M and λ ($K=0.4$, $Sc=1.0$, $Pr=1.0$, $Nt=0.1$, $Nb=0.1$).

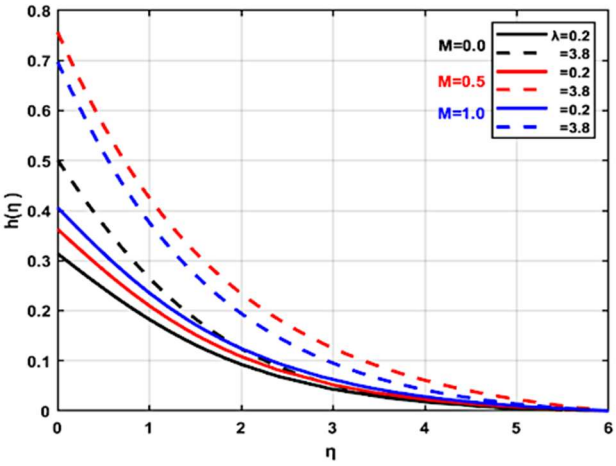

Fig.8. Microrotation profiles $h(\eta)$ for different values of M and. λ ($K=0.4$, $Sc=1.0$, $Pr=1.0$, $Nt=0.1$, $Nb=0.1$).

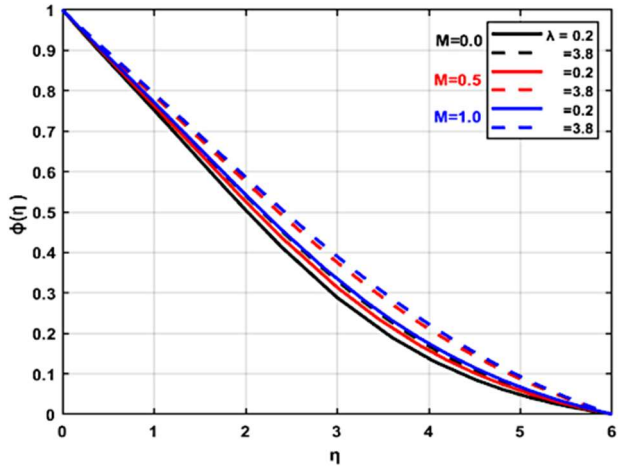

Fig.9. Concentration profiles $\phi(\eta)$ for different values of M and λ ($K=0.4$, $Sc=1.0$, $Pr=1.0$, $Nt=0.1$, $Nb=0.1$).

4.5. Effect of Brownian motion parameter Nb and material parameter K on the profiles

The Brownian parameter is random motion of nanoparticles due to collisions with molecules in the base- nanofluid. The coupling between Nb and microrotation makes the nanofluid behavior highly nonlinear and affects stability, heat transfer, and control of nanoparticle distribution. The micropolarity reduces the near-wall velocity gradient due to rotational torque while Brownian motion tends to higher gradients, as observed in Fig.10. Physically, the fluid's mixing is improved by the particles' random motion brought on by thermal

energy. Increased agitation helps distribute heat more uniformly, and leading to a higher temperature profile showed in Fig.11. In [22], the progression of the curves is the same. A competitive role is so observed between the Brownian motion of the nanoparticles and the additive viscosity generated by the micropolarity. Increasing Nb lead to thicker boundary layer, but the temperature gradient is better when K increases. Higher Nb values result in a more gradual decline in microrotation profile, Fig.12, indicating that Brownian motion helps sustain microrotational effects in the fluid. Brownian motion promotes particle diffusion while micropolarity can create rotation zones where concentration accumulates, are aspects of the profiles in Fig.13. This can lead to changes in viscosity and flow characteristics, which in turn affect thermal profiles and microrotation. Fick's rules govern particle movement from high to low concentration locations. Overall, Nb increases diffusion by enhancing particle mobility. In Fig.10. and Fig.12, no effect of varying Nb is found on f' and h' profiles for great K . Due to the slowdown caused by greater micropolarity or spin viscosity, the variations of Nb i.e. agitation, are whiteout effect on velocity and microrotation profiles.

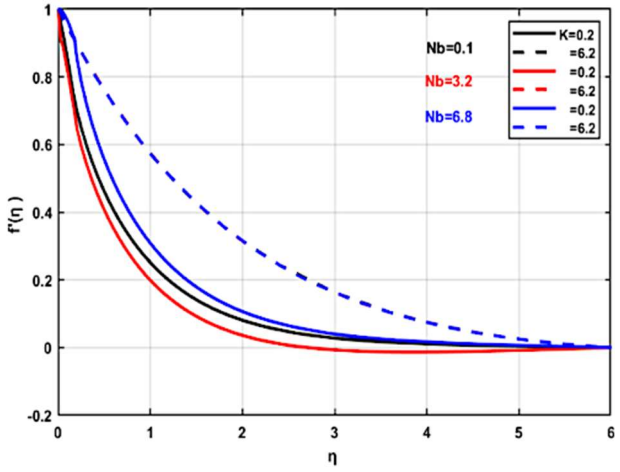

Fig.10. Velocity profiles $f'(\eta)$ for different values of Nb and K ($\lambda = 3.0$, $Sc = 1.0$, $Pr = 1.0$, $M = 0.4$, $Nt = 0.1$).

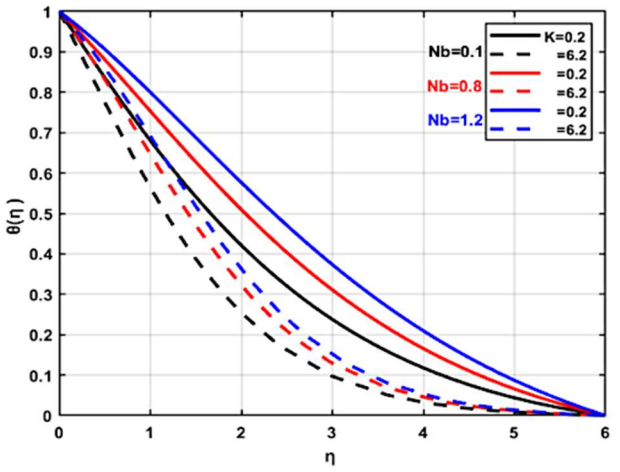

Fig.11. Temperature profiles $\theta(\eta)$ for different values of Nb and K ($\lambda = 3.0$, $Sc = 1.0$, $Pr = 1.0$, $M = 0.4$, $Nt = 0.1$).

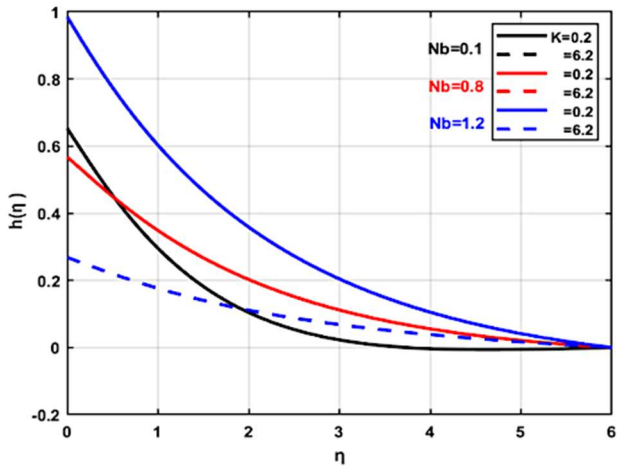

Fig.12. Microrotation profiles $h(\eta)$ for different values. of Nb and K ($\lambda = 3.0$, $Sc = 1.0$, $Pr = 1.0$, $M = 0.4$, $Nt = 0.1$).

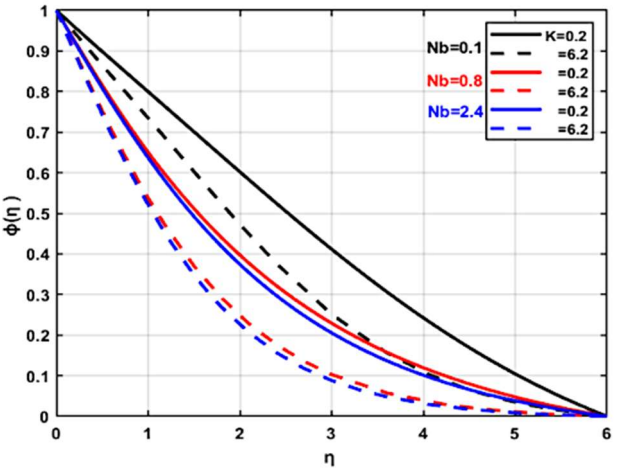

Fig.13. Concentration profiles $\phi(\eta)$ for different values of Nb and K ($\lambda = 3.0$, $Sc = 1.0$, $Pr = 1.0$, $M = 0.4$, $Nt = 0.1$).

4.6. Effect of Brownian motion parameter Nb and Williamson parameter λ on the profiles

The velocity profile $f'(\eta)$ in Fig.14 is impacted by the Williamson parameter λ et no effect of Nb is noted. Due to the variable viscosity the velocity is great at the sheet and weak in boundary layer center. The temperature profile is affected both by Nb and λ with heat redistributed according to areas of high Brownian activity and local viscosity, Fig.15. In Fig.16, at the sheet-nanofluid interface where the Brownian motion and the micropolarity are in competitive actions. Here as expected, in Fig.14 and Fig.16, no effect varying Nb is found on f' and h' for low values of λ behaving like a Newtonian nanofluid. The nanofluid remains generally stable in this case, since Nb has no impact on dynamic profiles. The concentration profile $\phi(\eta)$, in Fig.17, is influenced by the Brownian motion parameter Nb and the Williamson parameter λ. Increased Nb enhances particle dispersion. Higher Nb is equivalent to dispersion increases and $\phi(\eta)$ becomes more homogene. If λ increases, flow is strongly pseudoplastic and the particle distribution no longer follows the velocity field.

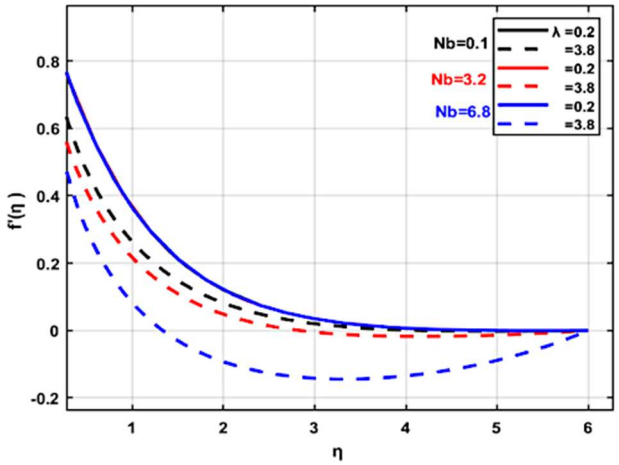

Fig.14. Velocity profiles $f'(\eta)$ for different values of Nb and λ ($K=0.4$, $Sc=1.0$, $Pr=1.0$, $M=2.0$, $Nt=0.1$).

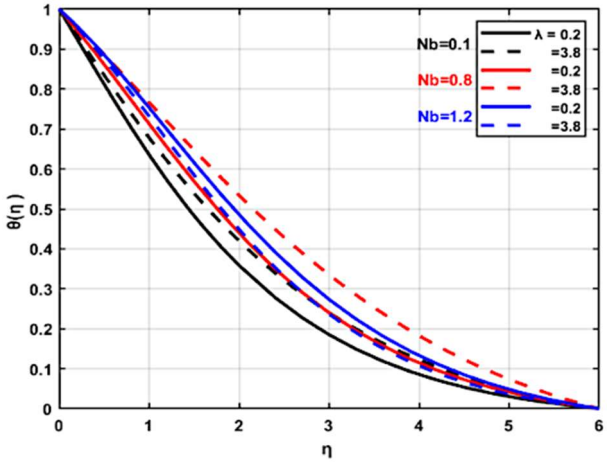

Fig.15. Temperature profiles $\theta(\eta)$ for different values of Nb and λ ($K=0.4$, $Sc=1.0$, $Pr=1.0$, $M=2.0$, $Nt=0.1$).

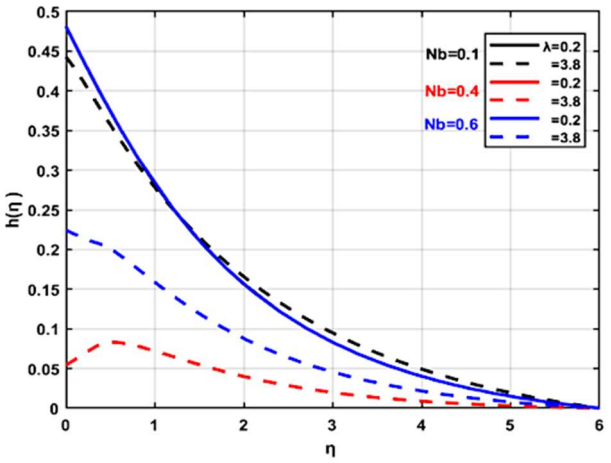

Fig.16. Microrotation profiles $h(\eta)$ for different values of Nb and λ ($K=0.4$, $Sc=1.0$, $Pr=1.0$, $M=2.0$, $Nt=0.1$).

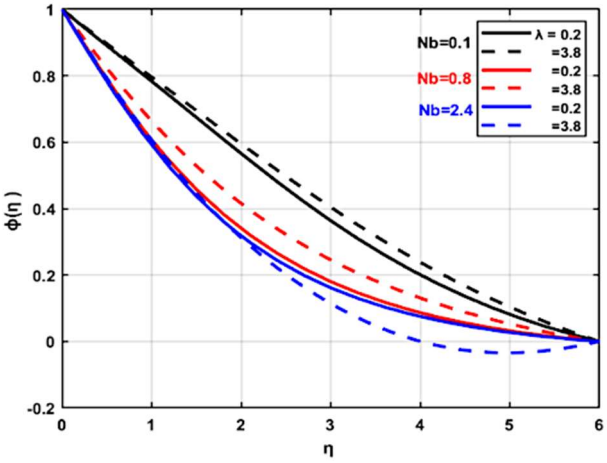

Fig.17. Concentration profiles $\phi(\eta)$ for different values of Nb and λ ($K=0.4$, $Sc=1.0$, $Pr=1.0$, $M=2.0$, $Nt=0.1$).

4.7. Effect of thermophoresis parameter Nt and material parameter K on the profiles

Nanoparticles migrate in a fluid under the effect of a temperature gradient and move from hot areas to cold areas. As expected, the thermophoresis parameter Nt changes do not affect the velocity profile. In Fig.18, only the material parameter have a substantial effect on this profile, as above explained. The thermophoresis parameter Nt significantly influences the effective viscosity of a fluid, impacting temperature profile $\theta(\eta)$ in Fig.19. As Nt increases, stronger thermophoretic forces drive particles toward cooler regions, towards a more uniform temperature distribution. By definition $Nt \approx \frac{1}{Nbt}$, the evolution is in agreement with [22]. The microrotation profile $h(\eta)$ is mostly affected by K, as one can see in Fig.20.

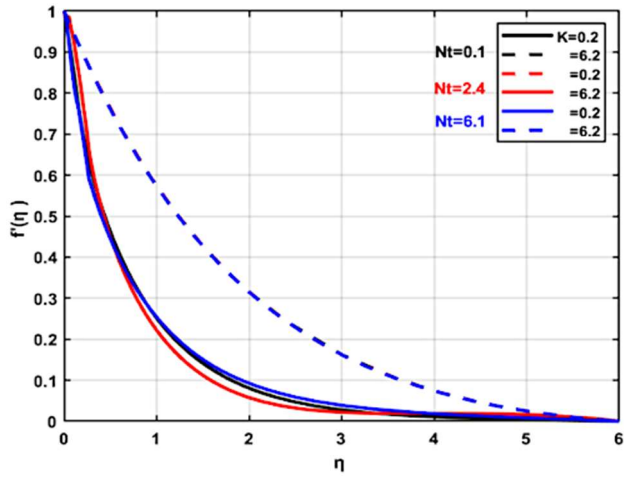

Fig.18. Velocity profiles $f'(\eta)$ for different values of Nt and K ($\lambda = 3.0$, $Sc = 1.0$, $Pr = 1.0$, $M = 2.0$, $Nb = 0.1$).

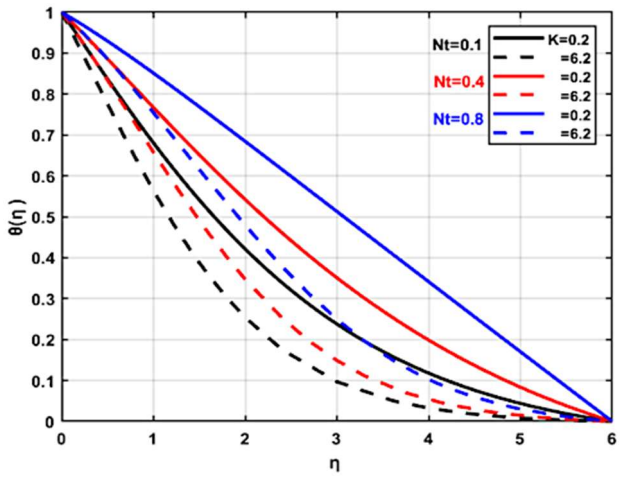

Fig.19. Temperature profiles $\theta(\eta)$ for different values of Nt and K ($\lambda = 3.0$, $Sc = 1.0$, $Pr = 1.0$, $M = 2.0$, $Nb = 0.1$).

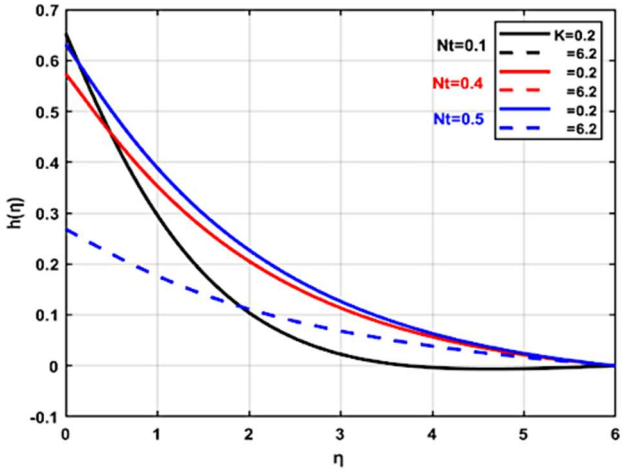

Fig.20. Microrotation profiles h(η)for different values Nt and K ($\lambda = 3.0$, $Sc = 1.0$, $Pr = 1.0$, $M = 2.0$, $Nb = 0.1$).

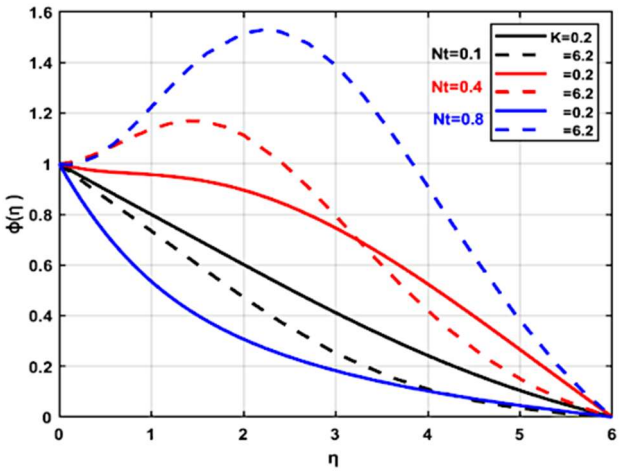

Fig.21. Concentration profiles $\phi(\eta)$ for different of Nt and K ($\lambda = 3.0$, $Sc = 1.0$ $Pr = 1.0$, $M = 2.0$ $Nb = 0.1$).

In contrast, the concentration profile $\phi(\eta)$ in Fig.21, is totally in dependence of Nt. It is interesting to note that very high nanoparticles concentration lies at $\eta = 2-3$ when thermophoresis phenomenon is strong. are the results of the interplay of viscosity, particle interactions, and flow dynamics. As before explained, in Fig.18. and Fig.20, no effect varying Nt i.e. migration, is found on f' and h' profiles for great K.

4.8. Effect of thermophoresis parameter Nt and Williamson parameter λ on the profiles

In Fig.22, the velocity $f'(\eta)$ is affected only by the Williamson parameter λ. The temperature profiles $\theta(\eta)$ represented in Fig.23, is influenced significantly both by the thermophoresis parameter Nt and by the change in the viscosity via the temperature.

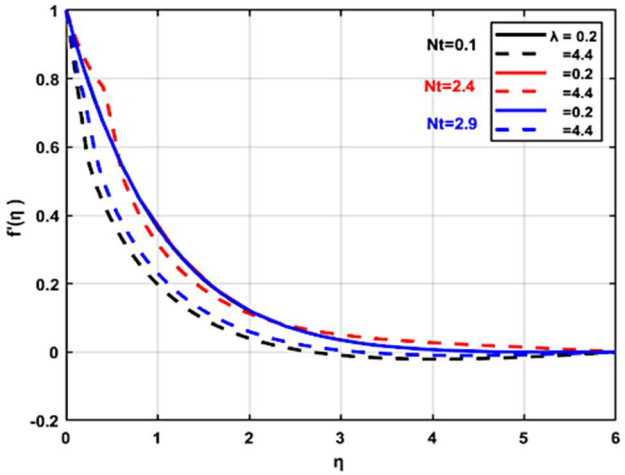

Fig.22. Velocity profiles $f'(\eta)$ for different values of Nt and λ ($K = 0.4$, $Sc = 1.0$, $Pr = 1.0$, $M = 2.0$, $Nb = 0.1$).

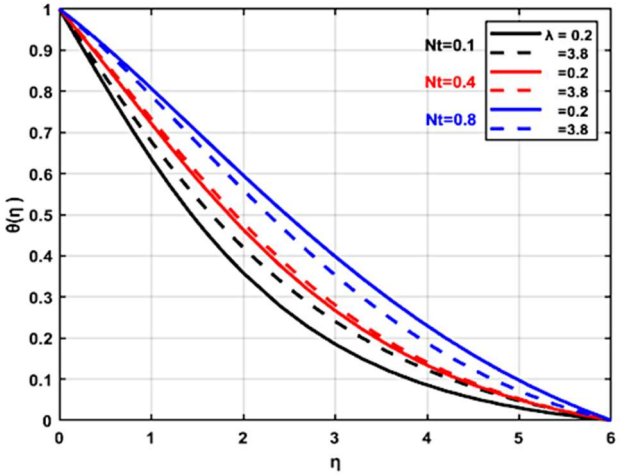

Fig.23. Temperature profiles $\theta(\eta)$ for different values of Nt and λ ($K = 0.4$, $Sc = 1.0$, $Pr = 1.0$, $M = 2.0$, $Nb = 0.1$).

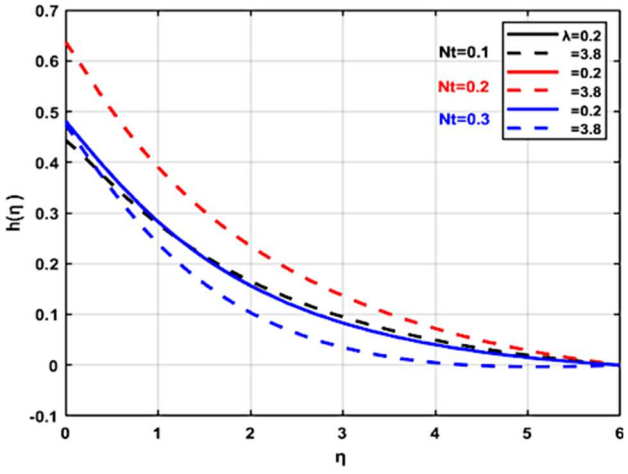

Fig.24. Microrotation profiles $h(\eta)$ for different values of Nt and λ ($K = 0.4$, $Sc = 1.0$, $Pr = 1.0$, $M = 2.0$, $Nb = 0.1$).

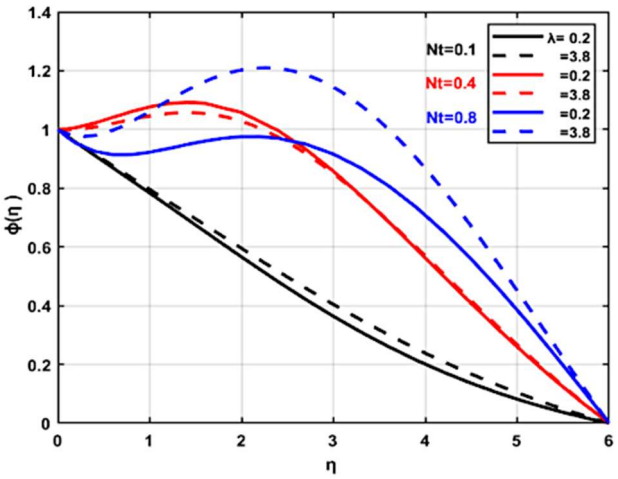

Fig.25. Concentration profiles $\phi(\eta)$ for different values of Nt and λ ($K = 0.4$, $Sc = 1.0$, $Pr = 1.0$, $M = 2.0$, $Nb = 0.1$).

More comprehensive fact that shows the complex interaction of the coupling. Similarly for the microrotation profile $h(\eta)$ presented in Fig.24. is in dependence with λ. For concentration profile $\phi(\eta)$, Fig.25, Nt as well as λ increase this profile change similarly as Fig.22, where a highly nonlinear curves with η are seen for high values of λ and Nt. As expected, in Fig.22 and Fig.24, no effect varying Nt is found change f' and h' for low values of λ.

4.9. Friction and heat transport quantities

The engineering quantities C_f and Nu_x are established and reported in Tab.2, following the values of f'', h and θ' at the stretching sheet-nanofluid interface and according to the corresponding values of the dimensionless numbers. From this table, a good reduction of the friction factor is observed using a Williamson fluid conjugated with a limited micropolarity. However, to enhance the heat transfer, it is recommended that the nanofluid base have a high Prandtl number. In the objective to dissipate more heat transfer, a good management consists to combine a nanofluid with moderate pseudoplasticity and micropolarity. These conditions ensure a better technical process.

Table 2. Effect of physical parameters on C_f and Nu number.

M	***K***	***λ***	***Sc***	***Pr***	***Nb***	***Nt***	***f″(0)***	***h(0)***	$R_{ex}C_f$	***-θ′(0)***
0.5	***2***	***0.3***	***1.0***	***3***	***0.15***	**0.15**	*–0.5625*	*0.2813*	*0.0159*	*0.7997*
0.0							*–0.4921*	*0.2461*	*0.0122*	*0.8112*
1.0							*–0.6253*	*0.3126*	*0.0194*	*0.7893*
	0.1						*–0.7872*	*0.3936*	*0.7168*	*0.3936*
	6.2						*–0.4051*	*0.2025*	*0.8586*	*0.8263*
		0.1					*–0.5595*	*0.2797*	***0.0051***	***0.8002***
		0.5					*–0.5657*	*0.2828*	*0.0265*	*0.7992*
			0.1				*–0.5625*	*0.2813*	*0.0159*	*0.8327*
			2.0				*–0.5625*	*0.2813*	*0.0159*	*0.7777*
				1.0			*–0.5625*	*0.2813*	*0.0159*	*0.3996*
				6.2			*–0.5625*	*0.2813*	*0.0159*	***1.2219***
					0.1		*–0.5625*	*0.2813*	*0.0159*	*0.8125*
					0.3		*–0.5625*	*0.2813*	*0.0159*	*0.7619*
						0.0	*–0.5625*	*0.2813*	*0.0159*	*0.9553*
						0.3	*–0.5625*	*0.2813*	*0.0159*	*0.6759*

5. Conclusions

A modeling and numerical simulations were conducted to analyse the impact of a magnetic field and Williamson micropolar-nanofluid flow on a nonlinear stretching plate, taking into account the micropolarity of the nanoparticles. The governing equations for this fluid are developed. Using the similarity method the partial differential equations are transformed into nonlinar ordinary differential equations. The result system is solved numerically using Lobatto III discretisation through bvp4c established program. Extensive results were get to show the effect of nanofluid rheology, nanoparticles, magnetic field and micropolarity on the velocities, microrotations, temperatures and volume fractions of nanoparticles profiles. It should be remarked that all profiles are highly dependent on the physics represented by various parameters and can complement each other or vice versa. The important findings of this paper are as flollows:

- The velocity gradient increases by increasing M . Higher K gives thicker velocity boundary layer. The combined increase of M and λ has the effect of increasing the velocity gradients.
- The temperature is raised sensibly by M for low values of K . Increased λ and M result in slower fluid flow, reduced mixing capabilities, does not greatly alter temperature distributions.
- The microrotation decreases largely with raising K near the stretching sheet. Its maximum value is reached with medium M and low K . Near the stretching sheet, high λ and M modify completely the profile.
- Little changes in the uniform concentration nanoparticles profiles with M while high K , λ and M makes the profile thickness thinner.
- Changes Nb and Nt have a substantial impact on the velocity gradient. K decreased the velocity gradient while it is increased by λ .
- The temperature boundary layer is strongly affected by Nb or Nt and less by K . On the other hand, λ have more impact on the corresponding profile than Nb or Nt variations.
- The microrotation is promoted by increasing Nb and Nt . Changes in this profile is important when λ varies.
- Raising λ , Nb or Nt modify the concentration of nanoparticules. The profile is more sensitive to the variations of Nb and Nt with low K and strong K , respectively.
- Using a Williamson fluid have a good reduction of the friction factor but increasing micropolarity is not beneficial.
- The improvement of heat transfer is confirmed for a nanofluid with high Prandtl number of the base-nanofluid.
- Under the present numerical conditions, the following values. $\left[M, K, \lambda, Sc, Pr, Nb, Nt\right] = \left[0.5, 2.0, 0.1, 1.0, 3.0, 0.15, 0.15\right]$ appear to be a good trade-off between reasonable heat exchange and less flow resistance.

These summarized results provides a motivation to highlight the entropy generated by this combination in order to minimized it. The objective will be to enable the designer plan for best conditions applied to industrial polymer sheet by extrusion.

Acknowledgements

This work was supported by the Biomaterials and transport phenomena laboratory agreement N° 303-03-12-2003, at University Yahia Fares of Medea, Algeria. All the authors acknowledge and gratefully thank the financial support provided by DG-RSDT of Algeria.

The authors are very much thankful to the reviewers for their constructive and valuable suggestions to improve the quality of the manuscript.

Nomenclature

$B(x)$ – magnetic field

B_0 – constant magnetic field

C – concentration of nanoparticles

Cf – skin friction coefficient

Cp – specific heat at constant pressure

D_B – Brownian diffusion coefficient

D_T – thermophoretic diffusion coefficient

f – dimensionless velocity

h – dimensionless microrotation

j – micro-inertia density
K – material parameter
Ln – nanofluid Lewis number
M – magnetic parameter
N – angular velocity or micro rotation
Nb – Brownian diffusion parameter
nf – nanofluid
Nt – thermophoretic diffusion parameter
Nu_x – local Nusselt number
Pr – Prandtl number
p – nanoparticle
Re_x – local Reynolds number
Sc – Schmidt number
Sh_x – local Sherwood number
T – temperature
U – constant velocity of the plate
u – velocity in x-direction
v – velocity in y-direction
w – at the wall
α – thermal diffusivity
β – volumetric thermal expansion coefficient
Γ – positive time constant
γ – spin gradient velocity
η – similarity variable
θ – dimensionless temperature
κ – spin viscosity
λ – Williamson nanofluid parameter
μ – dynamic viscosity
ν – kinematic viscosity
ρ – density
$(\rho c)f$ – heat capacity of the fluid
$(\rho c)p$ – effective heat capacity of the nanoparticule materiel
σ – electrical conductivity
φ – nanoparticle volume fraction
Ω – dimensionless temperature difference
∞ – out the boundary layer

References

[1] Williamson R.V. (1929): *The flow of pseudoplastic materials.*– Ind. Eng. Chem. vol.21, pp.1108-1111. https://doi.org/10.1021/ie50239a035.

[2] Bishnoi J., Kumar S. and Tyagi R. (2023): *Thermal convection of Rivlin-Ericksen fluid governed by the Brownian motion and thermophoresis of nanoparticles with passive behaviour of nanoparticles at the parallel boundaries.*– J. of Nanofluids, vol.12, No.5, pp.1194-1209. https://doi.org/10.1166/jon.2023.2010.

[3] Carapau F. (2008): *Axisymmetric motion of generalized Rivlin-Ericksen fluids with shear-dependent normal stress coefficients.*– Int. J. of Math. Models. Method . Appl. Sci., vol.2, pp.168-175. https://www.naun.org/main /NAUN/ijmmas/2008.htm.

[4] Nadeem S., Hussain S.T. and Lee C. (2013): *Flow of a Williamson fluid over a stretching sheet.*– Braz. J. Chem. Eng., vol.30, No.3, pp.619-625. https://doi.org/10.1590/S0104-66322013000300019.

[5] Nadeem S. and Hussain S.T. (2014): *Flow and heat transfer analysis of Williamson nanofluid.*– Appl. Nanosci., vol.4, pp.1005-1012. https://doi.org/10.1007/s10483-014-1807-6.

[6] Salawu S.O. (2023): *Stagnation-point flow of Williamson fluid along a stretched plate with convective thermal condition and activation energy.*– Int. J. of Applied Mechanics and Engineering, vol.28, No.3, pp.101-111. https://doi.org/10.59441/ijame/172900.

[7] Dey D. and Sahu D.S. (2021): *A review on the application of the nanofluids.*– Heat Transfer, vol.50, No.2, pp.1113-1155. https://doi.org/10.1002/htj.21920.

[8] Sharma A.K., Tiwari A.K. and Dixit A.R. (2016): *Rheological behaviour of nanofluids: A review.*– Renewable and Sustainable Energy Reviews, vol.53, pp.779-791. https://doi.org/10.1016/j.rser.2015.09.033.

[9] Anjali Devi S.P. and Mekala S. (2019): *Role of Brownian motion and thermophoresis effects on hydromagnetic flow of nanofluid over a nonlinearly stretching sheet with slip effects and solar radiation.*– Int. J. of Applied Mechanics and Engineering, vol.24, No.3. pp.489-508. https://doi.org/10.2478/ijame-2019-0031.

[10] Shahzad A., Liaqat F., Ellahi Z., Sohail M., Ayub M. and Ali M.R. (2022): *Thin film flow and heat transfer of Cu nanofluids with slip and convective boundary condition over a stretching sheet.*– Sci. Rep, vol.12, No.1, p.14254. https://doi.org/10.1038/s41598-022-18049-3.

[11] Saif R.S. and Muhammad T. (2023): *Melting heat transmission for nanoliquid flow through a curved stretching sheet with Darcy-Forchheimer phenomenon.*– Waves in Random and Complex Media, pp.1-21. https://doi.org/10.1080/17455030.2023.2193848.

[12] Waqas H., Farooq U., Hassan A., Liu D., Noreen S., Makki R., Hussain S. and Ali M.R. (2023): *Numerical and computational simulation of blood flow on hybrid nanofluid with heat transfer through a stenotic artery: Silver and gold nanoparticles.*– Results in Physics, vol.44, p.106152. https://doi.org/10.1016/j.rinp.2022.106152.

[13] Muhammad T. and Haider F. (2025): *Time-dependent flow of Reiner-Rivlin nanofluid over a stretching sheet with Arrhenius activation energy and binary chemical reaction.*– Multidiscipline Modeling in Materials and Structures, vol.21, No.1, pp.1-18. https://doi.org/10.1108/MMMS-05-2024-0123.

[14] Eid M.R. and Mabood F. (2021): *Entropy analysis of a hydromagnetic micropolar dusty carbon NTs-kerosene nanofluid with heat generation: Darcy-Forchheimer scheme.*– J. Therm. Anal. and Calorim., vol.143, pp.2419-2436. https://doi.org/10.1007/s10973-020-09928-w.

[15] Ramesh G.K., Roopa G.S., Rauf A., Shehzad S.A. and Abbasi F.M. (2021): *Time-dependent squeezing flow of Casson-micropolar nanofluid with injection/suction and slip effects.*– Int. Commun. Heat Mass Transfer, vol.126, p.105470. https://doi.org/10.1016/j.icheatmasstransfer.2021.105470.

[16] Almakki M., Mondal H. and Sibanda P. (2021): *Onset of unsteady MHD micropolar nanofluid flow with entropy generation.*– Int. J. Ambient Energy, vol.43, No.1, pp.43-56. https://doi.org/10.1080/01430750.2021.1890213.

[17] Reddy N.V.B., Kishan N. and Reddy C.S. (2019): *Melting heat transfer and MHD boundary layer flow of Eyring-Powell nanofluid over a nonlinear stretching sheet with slip.*– Int. J. of Applied Mechanics and Engineering, vol.24, No.1, pp.161-178. https://doi.org/10.2478/ijame-2019-0011.

[18] Kumar G.V., Varma S.V.K. and Kumar R.V.M.S.S.K. (2019): *Unsteady three-dimensional MHD nanofluid flow over a stretching sheet with variable wall thickness and slip effects.*– Int. J. of Applied Mechanics and Engineering, vol.24, No.3, pp.709-724. https://doi.org/10.2478/ijame-2019-0044.

[19] Khan M.W.A., Shah F., Khan M.I., Chu Y.M. and Kadry S. (2020): *Fully developed entropy-optimized MHD nanofluid flow by a variably thickened rotating surface.*– Appl. Phys. A, vol.126, pp.1-15. https://doi.org/10.1007/s00339-020-04068-2.

[20] Odesola A.S., Abiala I.O., Akinpelu F.O. and Fenuga O.J. (2020): *Analysis of magnetohydrodynamic (MHD) nanofluid flow with heat and mass transfer over a porous stretching sheet.*– Int. J. of Applied Mechanics and Engineering, vol.25, No.4, pp.162-174. https://doi.org/10.2478/ijame-2020-0056.

[21] Dang K., Makkar V. and Sharma N. (2021): *Numerical analysis of three-dimensional magnetohydrodynamics non-Newtonian free stream flow induced by permeable stretching surface.*– J. Ther. Eng, vol.10, No.6, pp.1465-1479. https://doi.org/10.14744/thermal.0000888.

[22] Ahmed K., McCash L.B., Akbar T. and Nadeem S. (2022): *Effective similarity variables for the computations of MHD flow of Williamson nanofluid over a non-linear stretching surface.*– Processes, vol.10, No.6, p.1119. https://doi.org/10.3390/pr10061119.

[23] Jauhri S. and Mishra U. (2022): *A study of MHD fluid with second order slip and thermal flow over a nonlinear stretching sheet.*– Int. J. of Applied Mechanics and Engineering, vol.27, No.2, pp.98-114. https://doi.org/10.2478/ijame-2022-0022.

[24] Kumar R.M., Raju R.S., Mebarek-Oudina F., Kumar M.A. and Narla V.K. (2024): *Cross-diffusion effects on an MHD Williamson nanofluid flow past a nonlinear stretching sheet immersed in a permeable medium.*– Frontiers in Heat and Mass Transfer, vol.22, No.1, pp.15-34. https://doi.org/10.32604/fhmt.2024.048045.

[25] Mesbah A., Allouaoui R., Bouaziz A.M. and Bouaziz M.N. (2024): *Entropy generation analysis of MHD micropolar-nanofluid flow over a moved and permeable vertical plate.*– Int. J. of Applied Mechanics and Engineering, vol.29, No.1. pp.73-89. https://doi.org/10.59441/ijame/175807.

[26] Iqbal J., Gul M. and Abbasi F.M. (2024): *Thermal transport of radially magnetized peristalsis of non-Newtonian nanofluid through an asymmetric curved channel.*– Numerical Heat Transfer, Part B: Fundamentals, pp.1-24. https://doi.org/10.1080/10407790.2024.2365905.

[27] Irfan M. and Muhammad T. (2024): *Numerical simulation of bio-convection radiative heat transport flow of MHD Carreau nanofluid.*– ZAMM-Journal of Applied Mathematics and Mechanics/Zeitschrift für Angewandte Mathematik und Mechanik, vol.104, No.11, e202300813. https://doi.org/10.1002/zamm.202300813.

[28] Iqbal J., Abbasi F.M. and Alam M.M. (2025): *Thermal enhancement in solar aircraft by using MHD Carreau Yasuda nanofluid with solar radiation.*– Aerospace Science and Technology, vol.158, 109906. https://doi.org/10.1016/j.ast.2024.109906.

[29] Iqbal J., Abbasi F.M. and Alam M.M. (2025): *Non-similar analysis for magnetohydrodynamic flow of hybrid nanofluid over a curved stretching surface with Hall current and viscous dissipation effects.*– Modern Physics Letters B, 2550145. https://doi.org/10.1142/S0217984925501453.

[30] Alouaoui R., Ferhat S. and Bouaziz M.N. (2024): *MHD and stability for convective flow of micropolar nanofluid over a moving and vertical permeable plate.*– Defect and Diffusion Forum, vol.408, pp.51-65. https://doi.org/10.4028/www.scientific.net/DDF.408.51.

[31] Vinodkumar Reddy M., Ajithkumar M., Zafar S.S.B., Faizan M., Ali F. and Lakshminarayana P. (2024): *Magnetohydrodynamic stagnation point flow of Williamson hybrid nanofluid via stretching sheet in a porous medium with heat source and chemical reaction.*– Proc. Inst. Mech. Eng., Part E: J. Process Mech. Eng. https://doi.org/10.1177/09544089241239583.

[32] Jangid S., Mehta R., Bhatnagar A., Alraddadi I., Alotaibi M.F. and Ahmad H. (2024): *Heat and mass transfer of hydromagnetic Williamson nanofluid flow study over an exponentially stretched surface with suction/injection, buoyancy, radiation, and more.*– Case Stud. Therm. Eng., vol.59, 104278. https://doi.org/10.1016/j.csite.2024.104278.

[33] Sharma K.R. and Jain S. (2024): *An unsteady MHD Williamson fluid flow in a vertical porous channel with porous media and thermal radiation.*– Int. J. Adv. Eng. Sci. Appl. Math., vol.16, pp.274-285. https://doi.org/10.1007/s12572-024-00371-w.

[34] Nabwey H.A., El-Hakiem A.M.A., Khan W.A., Abdelrahman Z.M, Rashad A.M. and Hawsah M.A. (2024): *Magnetic Williamson hybrid nanofluid flow around an inclined stretching cylinder with Joule heating in a porous medium.*– Chem. Eng. J. Adv., vol.18, p.100604. https://doi.org/10.1016/j.ceja.2024.100604.

[35] Chandan K.G., Mallikarjun B., Ghosh S.P. and Bhattacharyya S. (2024): *Entropy analysis for two-dimensional double-diffusive mixed convective flow of a Williamson nanofluid through a porous medium.*– Num. Heat Transfer, Part B: Fundamentals, vol.86, No.3, pp.1-21. https://doi.org/10.1080/10407790.2024.2329256.

[36] Butt Z.I., Raja M.A.Z. and Ahmad I. (2024): *Radial basis kernel harmony in neural networks for the analysis of MHD Williamson nanofluid flow with thermal radiation and chemical reaction: An evolutionary approach.*– Alexandria Eng. J., vol.103, pp.98-120. https://doi.org/10.1016/j.aej.2024.06.021.

[37] Rashad A.M., Nabwey H., Khan W.A. and Abdelrahman Z. (2024): *Heat and mass transfer of Oldroyd-B and Jeffery-Williamson ternary-hybrid nanofluids over a stretching sheet in a porous medium.*– J. Porous Media, vol.27, pp.25-49. https://doi.org/10.1615/JPorMedia.2024052406.

[38] Rashad A.M., Nafe M.A. and Eisa D.A. (2023): *Heat variation on MHD Williamson hybrid nanofluid flow with convective boundary condition and Ohmic heating in a porous material.*– Sci. Rep., vol.13, Article 6071. https://doi.org/10.1038/s41598-023-33043-z.

[39] Paul A., Mani Nath J.M. and Das T.K. (2023): *An investigation of the MHD Cu-Al2O3/H2O hybrid-nanofluid in a porous medium across a vertically stretching cylinder incorporating thermal stratification impact.*– J. .Therm. Eng., vol.9, No.3, pp.799-810. https://doi.org/10.18186/thermal.1300847.

[40] Jeelani M.B., Abbas A. and Alqahtani N.A. (2024): *Thermal transportation in heat generating and chemically reacting MHD Maxwell hybrid nanofluid flow past inclined stretching porous sheet in porous medium with solar radiation effects.*– Processes, vol.12, No.6, p.1196. https://doi.org/10.3390/pr12061196.

[41] Das T.K., Paul A. and Nath J.M. (2025): *Thermo-convection driven sodium alginate-based Darcy-Forchheimer EMHD Williamson hybrid nanofluid flow with varying thermal distribution.*– Mod. Phy. Lett. B, vol.39, No.05, p.2450405. https://doi.org/10.1142/S0217984924504050.

[42] Mohyuddin M.R. (2006): *On Solutions of Non-Linear Equations Arising in Rivilin-Ericksen Fluids.*– Doctoral Dissertation. Department of Mathematics, Quaid-i-Azam University, Islamabad PAKISTAN.

[43] Rivlin R.S. and Ericksen J.L. (1955): *Stress deformation relations for isotropic materials.*– J. Rat. Mech. Anal., vol.3, pp.323-425.

[44] Hsiao K.L. (2010): *Heat and mass transfer for micropolar flow with radiation effect past a nonlinearly stretching sheet.*– Heat Mass Transfer, vol.46, pp.413-419. https://doi.org/10.1007/s00231-010-0580-z.

[45] Bouaziz A.M., Bouaziz M.N. and Aziz A. (2021): *Influences of zero mass flux and active conditions on the predictions of double dispersion and double diffusive boundary layer in Darcy/non Darcy nanofluid flow.*– International Journal of Engineering Research in Africa, vol.57, pp.49-65. https://doi.org/10.4028/www.scientific.net/JERA.57.49.

[46] Yacob N.A. and Ishak A. (2011): *MHD flow of a micropolar fluid towards a vertical permeable plate with prescribed surface heat flux.*– Chem. Eng. Res. Des., vol.89, No.11, pp.2291-2297. https://doi.org/10.1016/j.cherd.2011.03.011

[47] Umar M., Amin F., Al-Mdallal Q. and Ali M.R. (2022): *A stochastic computing procedure to solve the dynamics of prevention in HIV system.*– Biomed. Signal Process. Control., vol.78, 103888. https://doi.org/10.1016/j.bspc.2022.103888.

[48] Mukdasai K., Sabir Z., Raja M.A.Z., Sadat R., Ali M.R. and Singkibud P. (2022): *A numerical simulation of the fractional order Leptospirosis model using the supervise neural network.*– Alex. Eng. J., vol.61, No.12, pp.12431-12441. https://doi.org/10.1016/j.aej.2022.06.013.

[49] Ali K.K., Tarla S., Ali M.R. and Yusuf A. (2023): *Modulation instability analysis and optical solutions of an extended (2+ 1)-dimensional perturbed nonlinear Schrödinger equation.*– Results in Phys., vol.45, 106255. https://doi.org/10.1016/j.rinp.2023.106255.

[50] Zafar A., Raheel M., Mahnashi A.M., Bekir A., Ali M.R. and Hendy A.S. (2023): *Exploring the new soliton solutions to the nonlinear M-fractional evolution equations in shallow water by three analytical techniques.*– Results in Phys., vol.54, 107092. https://doi.org/10.1016/j.rinp.2023.107092.

Received: February 7, 2025

Revised: February 24, 2026